1-^{11}C-Acetate Kinetics of Prostate Cancer

Christiaan Schiepers[1], Carl K. Hoh[2], Johan Nuyts[3], Marc Seltzer[1], Christine Wu[1], Sung-Cheng Huang[1], and Magnus Dahlbom[1]

[1]Molecular and Medical Pharmacology, David Geffen School of Medicine, University of California, Los Angeles, California; [2]Radiology, School of Medicine, University of California, San Diego, California; and [3]Nuclear Medicine, Katholieke Universiteit, Leuven, Belgium

^{18}F-FDG is in widespread use in cancer imaging but has limited utility in staging and monitoring of prostate cancer. 1-^{11}C-Labeled acetate, a substrate for the citric acid cycle, is superior. The kinetics of prostate tumors were investigated. **Methods:** Ten patients with primary prostate cancer, 10 with recurrent tumor, and 2 men with benign prostate hypertrophy were studied. After administration of 5.5 MBq/kg 1-^{11}C-acetate, dynamic PET of the pelvis was acquired for 20 min. Images were reconstructed with iterative algorithms, and corrections for attenuation and scatter were applied. Factor analysis produced factor images, representing iliac vessels and the prostate from which blood-input and tissue-output functions were derived with simple thresholding techniques. Five different kinetic models were applied to the dynamic data to estimate the rate constants. **Results:** The standard 3-compartment, 2-tissue model was able to describe 1-^{11}C-acetate kinetics of the prostate. The model could be reduced to 3 parameters by setting the tissue blood fraction and release from the second tissue compartment (k_4) to zero. Correction for metabolites appeared to be necessary. This reduced model performed marginally better than a 2-compartment model. A significant correlation was found between the influx rate constant (K) and acetate uptake (standardized uptake value) for primary tumors ($r = 0.91$), whereas there was no correlation for recurrent tumors ($r = -0.17$). Patlak graphical analysis provided accurate parameter estimates. **Conclusion:** A 3-compartment, 3-parameter model is able to describe adequately the acetate kinetics in prostate cancer. Significant differences between primary and recurrent cancer were found for transport k_1, influx K, distribution volume V_d, as well as early (6–10 min) and late (15–20 min) 1-^{11}C-acetate uptake.

Key Words: 1-^{11}C-acetate; PET; prostate cancer; benign prostate hypertrophy; kinetic modeling; factor analysis

J Nucl Med 2008; 49:206–215
DOI: 10.2967/jnumed.107.044453

Prostate cancer is common in the United States and the European Union and is the most frequently diagnosed cancer in men. Metabolic imaging with the glucose analog ^{18}F-FDG is a routine procedure in the imaging work-up and monitoring of cancer. For prostate cancer, ^{18}F-FDG is not suitable because of the physiologic excretion by the kidneys and the high concentration in the genitourinary (GU) tract. Dual-modality imaging with PET/CT would provide a possible solution, but prostate cancer usually has low glucose metabolism, making ^{18}F-FDG an ineffective radiopharmaceutical. Acetate is a substrate for the tricarboxylic acid (TCA) cycle and has <5% excretion into the GU tract. 1-^{11}C-Labeled acetate has been used for flow measurements, myocardial and lipid metabolism, and tumor imaging. Previously, we reported on the feasibility of using 1-^{11}C-acetate for imaging of prostate cancer (*1,2*) and performed dosimetry (*3*).

Dimitrakopoulou-Strauss and Strauss have written a concise editorial on the relevant issues of ^{18}F-FDG and 1-^{11}C-acetate in prostate cancer imaging (*4*). The radiopharmaceutical 1-^{11}C-acetate appears superior to ^{18}F-FDG in staging primary and recurrent prostate cancer (*5–7*). However, benign prostate hyperplasia (BPH) has similar uptake as malignant neoplasia (*4,8*), just as ^{18}F-FDG (*9*). Some of the discrepancies reported in the literature could be attributed to the acquisition protocol, static versus dynamic, and the timing of the images. Kato et al. (*8*) performed a dynamic acquisition in men with a normal prostate gland and found an age dependence of the acetate uptake. In addition, they found a similar acetate uptake in BPH and prostate cancer.

^{18}F-Labeled choline has also been proposed for prostate cancer (*10,11*). In a direct comparison of ^{18}F-choline and 1-^{11}C-acetate, Kotzerke et al. (*12*) demonstrated that both tracers performed nearly identically.

1-^{11}C-Acetate has been used to measure myocardial oxygen consumption, and the biochemical pathways are well known and have been published (*13–18*). In the current study, the 1-^{11}C-acetate kinetics of prostate cancer were evaluated with image-derived time–activity curves—that is, tracer clearance from the blood and uptake in the prostate (or prostate bed). Kinetic modeling was used to estimate the rate constants between the various compartments (Fig. 1). Multicompartment models were tested as were graphical analysis with Patlak plots (*19*). Metabolite and partial-volume corrections were applied to estimate 1-^{11}C-acetate transport across the cell membrane and influx into the tissue.

Received Jun. 21, 2007; revision accepted Nov. 19, 2007.
For correspondence or reprints contact: Christiaan Schiepers, MD, PhD, Molecular and Medical Pharmacology, David Geffen School of Medicine, AR-144 CHS, 10833 Le Conte Ave., Los Angeles, CA 90095-6942.
E-mail: cschiepers@mednet.ucla.edu

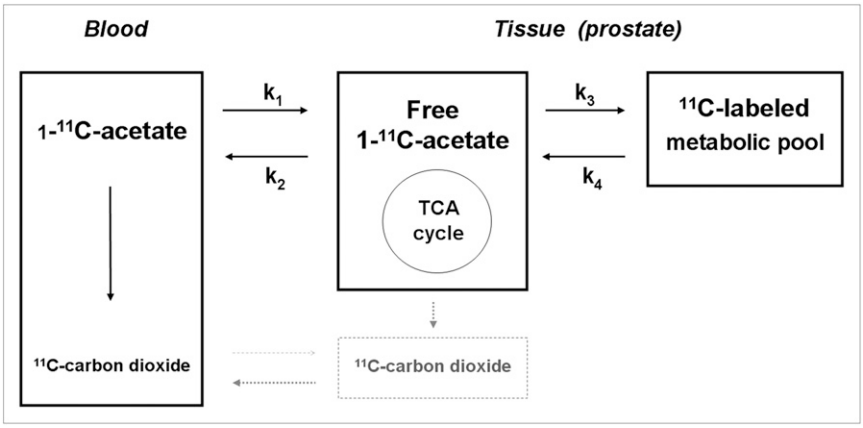

FIGURE 1. Kinetic model with 3 compartments and 2 tissues for prostate. CO_2 concentration in tissue is low because of low intracellular pH. In our simplified model, intracellularly labeled CO_2 (dotted gray box) is considered negligible. Blood-to-tissue transport is minimal as indicated by dotted gray arrow. Most of labeled CO_2 is transported rapidly to blood (as part of k_2). Metabolic pool consists of precursors for lipids, amino acids, fatty acids, and steroids that trap or retain ^{11}C label. Labeled products of tricarboxylic acid (TCA) cycle also contribute to metabolic pool (as part of k_3). Increase in TCA cycle metabolism would lead to increase of both k_2 and k_3.

MATERIALS AND METHODS

Patients

The study population consisted of 22 men: 10 with primary prostate cancer, 10 with a prostate-specific antigen (PSA) relapse after radical prostatectomy (recurrent cancer), and 2 with BPH. The average age was 65 y (range, 48–79 y). The Gleason score in primary cancer was, on average, 7.6 (median, 7.5) and was 7.1 (median, 7.0) for the recurrent cancer group. Serum PSA was, on average, 22.2 mg/mL (range, 4–75 mg/mL) for primary cancer, 12.7 mg/mL (range, 1–68 mg/mL) for recurrent cancer, and 1.4 mg/mL for BPH. The PSA velocity for the group with recurrent cancer (PSA relapse) was, on average, 3.0 mg/mL/mo (median, 0.4 mg/mL/mo; range, 0.1–16.1 mg/mL/mo). All subjects had fasted at least 6 h before imaging.

This study was approved by the local Office for Protection of Research Subjects and the Institutional Review Board (IRB) of the University of California at Los Angeles (UCLA), and all patients signed an informed consent to participate in the imaging study.

Image Acquisition

1-^{11}C-labeled acetate was synthesized according to a previously reported procedure (*20,21*). A dose of 5.5 MBq/kg (0.15 mCi/kg) 1-^{11}C-acetate was administered intravenously. PET was performed using an ECAT HR or HR+ system (Siemens Medical Solutions, Inc.). A transmission scan of 20-min duration was acquired first, in 2-dimensional (2D) mode. Subsequently, 1-^{11}C-acetate was administered intravenously, and a dynamic acquisition was begun simultaneously in 2D mode. Twenty-eight frames were acquired of 12 × 10, 9 × 20, 5 × 60, and 2 × 300 s duration.

The images were reconstructed with iterative techniques, maximum a-posteriori maximization (MAP) (*22,23*) for the transmission scan and (ordered-subset maximum likelihood expectation maximization [OSEM] consisting of the following sequence of iterations and subsets: 1–16, 1–12, 1–4, 2–1) (*24* and Supplemental Appendix [supplemental materials are available online only at http://jnm.snmjournals.org]) for the emission scan. Corrections for attenuation and scatter were applied. A gaussian kernel with 6-mm full width at half maximum was used as the postreconstruction smoothing filter. To get the same *x*- and *y*-pixel size, a zoom of 1.5 was used for the ECAT HR+ and 1.28 was used for the HR image reconstruction. The final volume-set had a matrix size of 128 × 128 and consisted of 47 (ECAT HR) or 63 (ECAT HR+) planes, resulting in a voxel size of 3.375 × 3.375 × 3.125 or 3.375 × 3.375 × 2.425 mm^3, respectively.

Processing

Factor analysis (FA) was performed on the volume set of reconstructed images (*2*). To speed up processing, data were resampled into larger voxels by zooming, plane summation, and rebinning, yielding a nearly isometric dataset of 13.5 × 13.5 × 12.5 mm^3 voxels (ECAT HR) or 13.5 × 13.5 × 12.1 mm^3 voxels (ECAT HR+) that was used for further processing (Supplemental Appendix). Time–activity-curves were generated for every voxel within the pelvis, and FA with a positivity constraint was applied. For our implementation, 3 factors and their corresponding factor images were generated. Factor 1 represented the arterial structures, factor 2 the prostate, and factor 3 the remainder. Tumor was seen in the second factor image. A volume of interest (VOI) was created by simple thresholding of the corresponding factor images. For the iliac vessels, a threshold of 50% was used, which is usual at our institution, and for the tumors 50% was used. With the created VOI, an image-based time–activity curve was generated from the reconstructed dynamic dataset. The time–activity curve from the iliac vessels served as the blood curve, and the time–activity curve for tumor or prostate served as the tissue curve. After correcting these time–activity curves for partial-volume effects, they were used as input and output functions for kinetic modeling. There were 20 patients with cancer (10 primary and 10 recurrent), and 2 men without cancer (BPH). Thus, 22 time–activity curve pairs were available for analysis.

Kinetic Model

The complete model for myocardial 1-^{11}C-acetate kinetics based on known biochemical pathways was published previously (*13,14,25,26*). For the prostate, the kinetic model has not been elucidated. Some consider the increased citrate oxidation in the TCA cycle in neoplasms as the cause of enhanced acetate uptake (*27*), based on the view of the prostate as a citrate-producing gland (*28*). Others attribute the increased uptake to acetate retention in the prostate due to enhanced lipid synthesis (*4*), whereas the contribution as precursor (e.g., to amino and fatty acids, steroids) is usually not considered (*29*). In the current approach, our previously published myocardial model was adapted to the standard 3-compartment, 2-tissue model in oncology (Fig. 1), as is generally used for ^{18}F-FDG (*30,31*). Briefly, acetate is transported across the cell membrane and used as substrate for various intracellular processes—for example, inside mitochondria for energy metabolism, and in the cytosol for enhanced lipid synthesis, building-blocks for membranes, amino acids, and steroids. The incorporation into lipids, amino acids, and so forth has a

turnover in the order of hours. Given our acquisition time of just 20 min, possible pathways are oxidation in the TCA cycle to CO_2 and H_2O and intracellular pooling for further metabolization.

Kinetic modeling using 3 compartments, as shown in Figure 1, yielded the 4 rate constants k_1, k_2, k_3, and k_4 (min^{-1}), from which the influx rate constant K was calculated as $k_1 \cdot k_3 \ (k_2 + k_3)^{-1}$ (min^{-1}). The blood volume fraction in tissue was estimated as a fifth parameter, V_b (Supplemental Appendix). This 3-compartment 5-parameter (3C-5p) model was subsequently simplified by reducing the number of parameters (setting them to 0). This is similar to van den Hoff et al., who validated a simple 3-compartment. 3-parameter (3C-3p) model for the acetate metabolism of the myocardium (*16*). Further reduction yielded a 2-compartmental model, which estimated 2 rate constants plus the blood volume fraction in tissue V_b. The effects of correction for metabolites and partial volume were investigated. Subsequently, Patlak graphical analysis was performed to estimate the influx rate constant K_{Patlak} and the distribution volume V_{Patlak}.

Contrary to prior studies, no metabolites were measured. Instead, the data of other publications were used. Although the metabolic rate of prostate cancer may be low, significant amounts of CO_2 are present in blood from tissues with active oxidative metabolism, which contaminate the input function (^{11}C-CO_2; Fig. 1). Both Buck et al. (*15*) and van den Hoff et al. (*32*) have shown that the metabolites from acetate in the blood follow a monoexponential function:

$$\text{Metabolite fraction} = a\,\{1 - e^{-(\ln 2/T_{1/2})(t - t_0)}\}. \qquad \text{Eq. 1}$$

The main difference between the published formulae concerns the time shift t_0 used by van den Hoff et al. and constant $a = 0.91$ used by Buck et al. Because the metabolites appear after a short delay, the van den Hoff equation was used here—that is, $a = 1$, $T_{1/2} = 6.69$, and $t_0 = 0.48$ min:

$$\text{Metabolite fraction} = 1 - e^{-0.104(t - 0.48)} \ \text{for} \ t > 0.48\,\text{min}. \qquad \text{Eq. 2}$$

It turned out that for our data, Equation 2 produced somewhat better fits than the Buck equation. At 15 min, the metabolites comprise approximately 80% of the activity in the vascular compartment.

Statistical Analysis

Results are presented as the mean ± 1 SD. Nonparametric tests were used to compare parameters between subgroups because of sample size—that is, the Sign test and the Wilcoxon–Mann–Whitney *U* test. Linear regression analyses were used to study the correlation between parameters, subgroups, tumor types, and patients. Differences between kinetic models were analyzed with the F test to correct for the different number of parameters involved in the various models (*33,34*). The Akaike information criterion (AIC) was calculated to directly compare the different models. The AIC is based on the concept of entropy and is a measure of the goodness of fit of an estimated statistical model. In the general form for normally and independently distributed model errors:

$$AIC = 2\,N_p + N_i \ln\,(RSS/N_i), \qquad \text{Eq. 3}$$

with N_p the number of parameters, N_i the number of observations, and RSS the residual sum of squares between measured and model parameters. This AIC penalizes overfitting of data (*35*).

RESULTS

FA was successful in all 22 cases. Figure 2A displays typical images of factor 1, representing the vascular structures—for example, the iliac arteries—and Figure 2B shows the corresponding maximum-intensity-projection (MIP) image. Figure 2C shows the factor images of a prostate gland with a primary tumor, and Figure 2D shows the corresponding MIP image. Three factors were established, and the iliac vessels and the prostate were easily identified in factor 1 and factor 2, respectively. In one study, the prostate was not found in factor 2, but in factor 3, which turned out to be a BPH patient with unusually high uptake of acetate in the bowel. The 3 factors accounted for an explained variance of 83% ± 9% (range, 66%–95%). Factor 1 contributed, on average, 67% and factor 2 contributed, on average, 11%. The number of voxels available for the iliac vessels was similar for the 3 subgroups (21 ± 8). The number of tissue voxels (tumor/prostate) was smaller for both primary cancer and BPH (44 ± 47) compared with that for recurrent tumors (157 ± 145), underscoring the generally stronger signal (i.e., higher uptake) of primary cancer and benign hyperplasia.

VOIs were created from the factor images and time–activity curves generated; typical examples of uptake curves are shown in Figure 3. One of the patients had significant bladder uptake, and image planes had to be constrained to define the prostate. This patient was suspected of having cystitis, but there was no clinical evidence at the time of the study. Two patients had some tracer in the urethra, but the mask of the thresholding algorithm was sufficient to delineate the prostate gland. One patient had high small-bowel uptake, and approximately half of the patients showed significant uptake in the rectum. In all cases, the bowel was at a sufficient distance from the prostate for accurate delineation. Time–activity curves of the vessels and tissues had the following area-under-the-curve (AUC): 24.6 ± 3.8 for the iliac arteries and 46.6 ± 8.6 for the tumor/prostate.

1-^{11}C-Acetate Tumor Kinetic Model

Compartmental models were used to estimate the kinetic parameters of the prostate tumors, and the average results are shown in Table 1. As an error estimate, the weighted residual sum of squares (WRSS) was calculated—that is, (fitted − measured value)^2 weighted by frame duration:

$$WRSS = \sum_{i=1}^{28} \left(Y_i^{\text{fitted}} - Y_i^{\text{measured}}\right)^2 \times (\text{duration frame}_i/\text{maximum frame duration}). \qquad \text{Eq. 4}$$

Reduction of the number of parameters involved did not have a dramatic impact on individual parameter estimates. The AIC showed that a 2-compartment model is insufficient to describe the data. The AIC appeared the lowest for

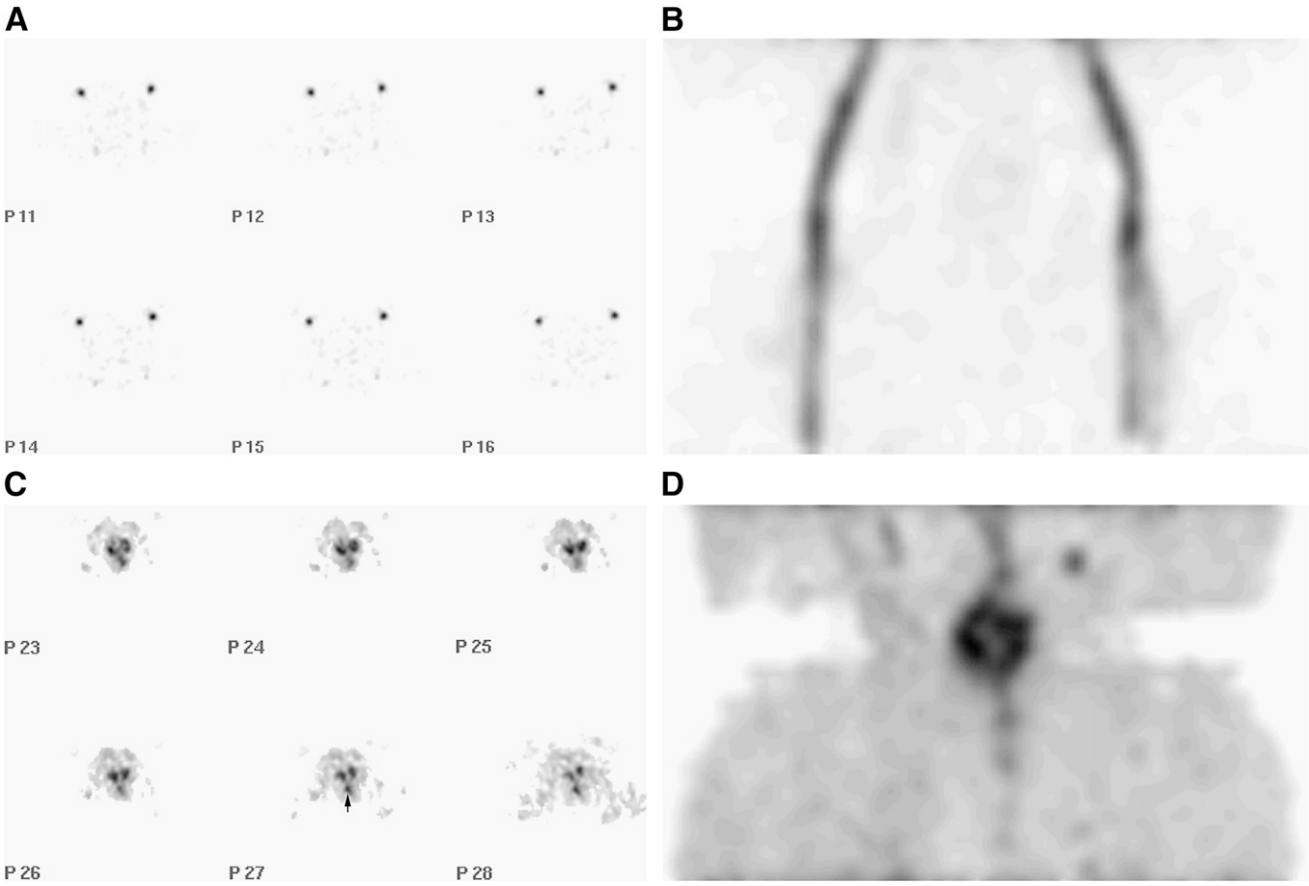

FIGURE 2. Parametric images from 65-y-old man with primary prostate cancer. (A) Factor images representing vascular component; right and left iliac arteries are identified in 6 transverse planes. (B) Maximum-intensity-projection image of factor 1 in anterior–posterior view representing iliac arteries. (C) Transverse factor images representing tumor component. Note bilobular involvement. Arrow points to tracer in rectum. (D) Maximum-intensity-projection image of factor 2 in anterior–posterior view showing prostate. Note hot spot, left and superior of prostate, represents metastatic lymph node.

the 3C-5p and 3C-3p models using metabolite correction. Reducing the number of parameters in the model from 4 to 3 showed a significant decrease in the AIC for 19 cases ($P < 0.01$ Sign test) and reduction from 5 to 3 parameters showed a decrease in 16 cases ($P < 0.05$ Sign test). The tissue blood fraction V_b is small and can easily be ignored as demonstrated in Table 1. A similar reasoning holds for k_4. Corrections for partial volume are obviously necessary given the 4- to 7-mm size of the iliac arteries. Partial-volume correction for the blood curve mainly affects k_1 and, therefore, the influx rate constant K. As reported previously (*2*), a recovery coefficient of 0.6 was selected for the vascular time–activity curve. To investigate the partial-volume effects for the output function in more detail, the volume of the tumor/gland was determined by adding all voxels within the VOI. The average volume was 12.5 ± 6.8 mL for primary cancer, 13.9 ± 10.3 mL for recurrent cancer, and 9.4 ± 6.2 mL for BPH. Assuming a sphere, the overall average volume of 12.8 mL translates to a diameter of 29.1 mm, which is >4 times the spatial resolution of our scanners. Therefore, 1.0 was selected as the recovery coefficient for the time–activity curve of tumor/prostate.

Metabolite correction improved the tightness of the fits and reduced the error estimates. Most of the individual error estimates did not differ significantly; Table 1 denotes the exceptions. However, the error estimate for each model was lower with metabolite correction than without metabolite correction ($P < 0.001$ Sign test). The same is true for the AIC, which appeared consistently and for every patient lower for each specific model with versus without metabolite correction ($P < 0.01$ Sign test). Moreover, the influx rate constant K has a more realistic value with metabolite correction. Direct comparison of the 3C-3p versus the 2C-3p model revealed significant differences ($P < 0.001$) for 6 patients with the F test (*34*); group comparison was significantly different with both the Sign test and the *U* test ($P < 0.01$). Reducing the number of parameters in the model to 3 showed a decrease in the AIC for most cases. Thus, it appears that a 3-compartment, 3-parameter model with metabolite and partial-volume correction is adequate and sufficient to describe acetate kinetics in prostate cancer. Patlak graphical analysis produced similar results, and K_{patlak} was close to K estimated with nonlinear regression. The distribution volume estimated with the Patlak plot was

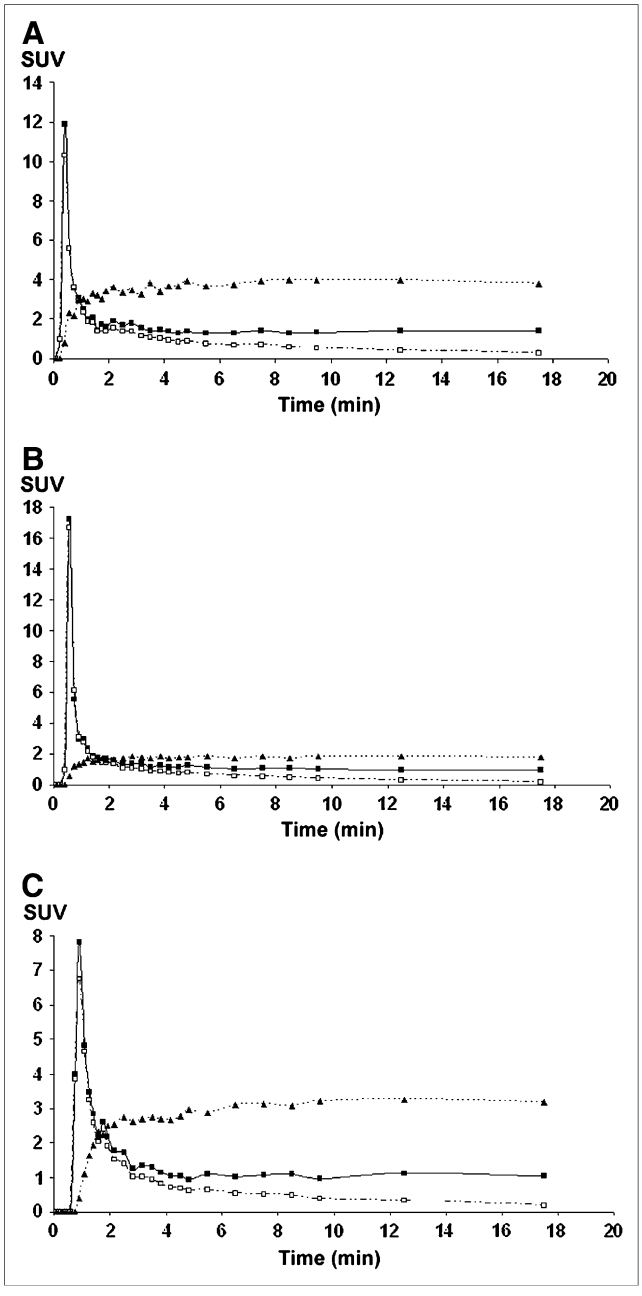

FIGURE 3. Time–activity-curves from iliac arteries (squares, solid line), metabolite-corrected input function (open squares, dashed line), and prostate tumor (triangles, dotted line). Uptake is expressed in SUV (standardized uptake value). (A) A 65-y-old man with primary prostate cancer (patient in Fig. 2). (B) A 57-y-old man with recurrent cancer; note lower SUV of tumor. (C) A 49-y-old volunteer with BPH.

also within the range of modeling values, and no significant differences were found (Tables 1 and 2).

Results of the parameters per subgroup in Figure 4 show a significant difference between primary and recurrent cancer for k_1 and K but not for k_2 and k_3. K_{patlak} also turned out to be significantly different for primary versus recurrent cancer. The relation between the influx rate K and the transport rate k_1 is linear as shown in Figure 5, although the range for recurrent tumor is much smaller than that for primary cancer.

1-^{11}C-Acetate Uptake Patterns

The tissue curve has a steep initial incline (Fig. 3) and approaches a plateau, reaching the maximum around 5 min. Analysis of the individual time–activity curves revealed that the early uptake (SUV-early), from 6 to 10 min, was, on average, similar to the late uptake, from 15 to 20 min (Table 2). None of the early-to-late ratios was significantly different from unity. Subgroup analysis revealed that there was significantly different uptake in primary versus recurrent prostate cancer with SUV-late 3.84 versus 1.91 ($P < 0.001$), respectively. The range of SUV-late was 1.8–5.5 for primary cancer, 1.5–2.6 for recurrent cancer, and 3.2–3.5 for BPH. The difference between BPH and recurrent cancer was significant ($P = 0.02$) but primary cancer could not be differentiated from BPH. A linear relationship between influx rate K and SUV-late was found for primary tumors ($r = 0.91$), but not for recurrent cancer ($r = -0.17$) (Fig. 6).

DISCUSSION

In this study, the kinetics of 1-^{11}C-acetate in prostate cancer and BPH were investigated, and the compartment model selected was that which described the data best. Our way of analysis is completely image-based and has minimal operator dependency. The FA takes all voxels within the visualized pelvis into account. The factor images are parametric images, representing structures of interest with similar activity changes as a function of time. The thresholding algorithm will automatically create the VOI in *x*-, *y*-, and *z*-dimensions from the factor images and generate the time–activity curves from the dynamic dataset. Uptake in the bladder posed a problem in 1 study. Although uptake in the rectum and the bowel was seen in most patients, the tomographic images were able to distinguish the structures easily in the spatial domain.

In the past, we have demonstrated that FA can reliably generate an input function for various radiopharmaceuticals and organ systems (*1,2,36*). These studies have shown that kinetic parameters obtained with an FA-based input function are similar to those obtained with a sampled blood curve, and no statistically significant differences were found for the rate constants obtained with these time–activity curves. The use of FA as an "intrinsic" way to correct for partial-volume effects and methods to calibrate the input function were published elsewhere (*37*).

Corrections for metabolites and partial volume are necessary to produce an adequate fit between the measured and model-generated time–activity curve. Measuring the metabolites in blood allows one to individualize the correction, which is obviously superior. However, 2 theoretic methods have been published (*15,32*). We used the equation of van den Hoff et al. (Eq. 2) (*32*) to correct for the metabolites in blood and to generate a realistic input function. Another method is to "calibrate" or "scale" the metabolite curve

TABLE 1
Kinetic Modeling of Prostate

Parameter	3C-5p	3C-5p	3C-4p	3C-4p	3C-3p	3C-3p	2C-3p	2C-3p	Patlak-2p	Patlak-2p
Metabolite correction	No	Yes	No	Yes	No	Yes	No	Yes	No	Yes
n	22	22	22	22	22	22	22	22	22	22
k_1	0.289 ± 0.130	0.318 ± 0.145	0.301 ± 0.131	0.319 ± 0.142	0.295 ± 0.134	0.316 ± 0.145	0.289 ± 0.132	0.231 ± 0.099		
k_2	0.190 ± 0.051	0.184 ± 0.108	0.206 ± 0.054	0.216 ± 0.091	0.190 ± 0.047	0.202 ± 0.100	0.177 ± 0.046	0.048 ± 0.013		
k_3	0.006 ± 0.010	0.126 ± 0.078	0.012 ± 0.018	0.141 ± 0.046	0.005 ± 0.008	0.124 ± 0.046				
k_4	0.002 ± 0.002	0.008 ± 0.008	0.008 ± 0.017	0.006 ± 0.004						
K	0.006 ± 0.010	0.124 ± 0.062	0.012 ± 0.013	0.124 ± 0.049	0.006 ± 0.008	0.118 ± 0.049			0.005 ± 0.011	0.109 ± 0.056
V_b	0.020 ± 0.020	0.024 ± 0.026					0.001 ± 0.003	0.000 ± 0.001		
V_d	1.52 ± 0.63	1.50 ± 1.28	1.44 ± 0.67	0.96 ± 0.46	1.53 ± 0.59	1.08 ± 1.03	1.62 ± 0.60	4.87 ± 1.80	1.51 ± 0.61	1.57 ± 1.50
WRSS	397 ± 420	295 ± 278	439 ± 448	376 ± 368	491 ± 478	372 ± 386	491 ± 470	852 ± 722		
N_F	0	9	1	6	0	4	Reference M−	Reference M+		
AIC	71 ± 28	65 ± 26	72 ± 28	68 ± 28	74 ± 28	66 ± 28	75 ± 27	92 ± 24		

2C, 3C = number of compartments; 2p, 3p, 4p, 5p = number of parameters in model. In model 3C-4p, $V_b = 0$ and in model 3C-3p both V_b and k_4 are fixed to 0. N_F = number of studies with a significantly lower error compared with corresponding 2C-3p (M− and M+—i.e., without and with metabolite correction as reference) determined with F test ($P < 0.05$). AIC (Akaike Information Criterion) is defined in Equation 3, and WRSS was used to calculate the likelihood function (*35*).

Estimates of fitted parameters k_1–k_4, as well as influx rate constant K, V_b, and V_d. Results are expressed as mean ± 1 SD of 22 studies (*n*) in 22 patients. Input function was corrected for partial-volume effects with 0.6 as recovery coefficient and for metabolites as indicated. Error estimate WRSS (Eq. 4) is a measure of "goodness of fit" between measured and calculated output function. Graphical analysis with Patlak plots was applied on images between 7 and 20 min.

TABLE 2
Three-Compartment, 2-Tissue Model with 3 Parameter Estimates, k_1–k_3, Influx Rate Constant K, and Distribution Volume V_d

Type	Primary Cancer	Recurrent cancer	P	BPH
n	10	10		2
k_1	0.419 ± 0.136	0.208 ± 0.073	<0.001	0.339 ± 0.050
k_2	0.218 ± 0.074	0.202 ± 0.124	NS	0.122 ± 0.066
k_3	0.120 ± 0.026	0.140 ± 0.054	NS	0.066 ± 0.058
K	0.152 ± 0.051	0.086 ± 0.017	<0.01	0.110 ± 0.049
V_d	1.25 ± 0.32	0.69 ± 0.27	<0.001	2.19 ± 1.18
Patlak K	0.137 ± 0.062	0.079 ± 0.035	0.02	0.121 ± 0.048
Patlak V_d	1.95 ± 1.67	1.00 ± 1.27	NS	2.49 ± 1.22
SUV-early	3.80 ± 0.99	1.83 ± 0.40	<0.001	3.55 ± 0.60
SUV-late	3.84 ± 1.07	1.91 ± 0.34	<0.001	3.35 ± 0.24

NS = not significant.

Patlak plot results are given, as well. Results are expressed as mean ± 1 SD for 3 different tissue types. 1-^{11}C-Acetate uptake at early (6–10 min) and late (15–20 min) time points is presented in SUVs. *P* denotes significance level by comparison of primary vs. recurrent cancers.

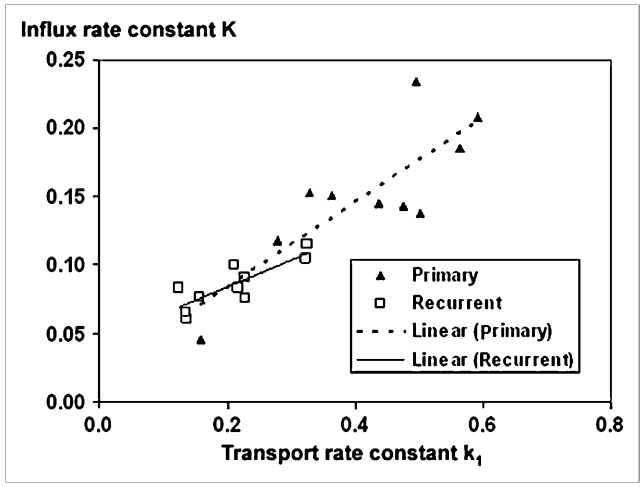

FIGURE 5. Scatter diagram of transport rate constant k_1 vs. influx rate constant K, both in min^{-1}. Triangles indicate primary cancer and open boxes indicate recurrent cancer. Lines are results of linear regression analysis, $r = 0.82$ (black) and $r = 0.84$ (gray). Slopes of linear fits are not statistically different.

with a late blood sample. We have used this technique in previous work (*1,2,36,37*) but not in the current experiments. It should be noted that the concentration of labeled CO_2 is relatively low, as the blood is moving continuously and it is exhaled via the lungs. Assuming that the interindividual blood activity concentrations have a low variation coefficient allows one to use an analytic function for the metabolite correction. The CO_2 level in tissue is a factor of 2.5 lower than that in blood because of the lower intracellular pH (*38*). In our model, the labeled CO_2 pool in tissue was considered negligible and was ignored (Fig. 1). More research is needed to provide evidence for these assumptions. Possible variations due to food intake were controlled by imaging individuals after prolonged fasting.

Partial-volume correction was applied by using a recovery coefficient of 0.6 for the blood curve. This choice was based on the iliac artery size of 4–7 mm and on recovery coefficients determined for our PET system based on earlier work (*2,39*). For the output function we used a recovery coefficient of 1 because the tumors were, on average, >10 mL. With dual-modality scanners (PET/CT), correction for

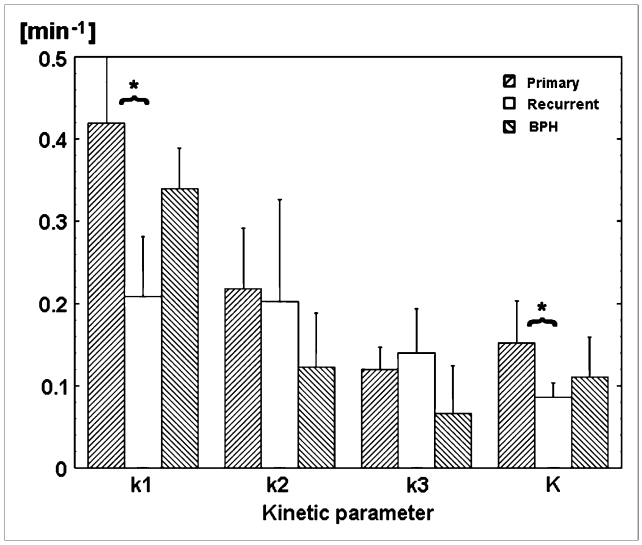

FIGURE 4. Average values of kinetic parameters for 3 subgroups: primary and recurrent cancer as well as BPH. Error bar denotes 1 SD. Primary and recurrent prostate cancer show significant differences (*$P < 0.01$) for k1 and K (Table 2).

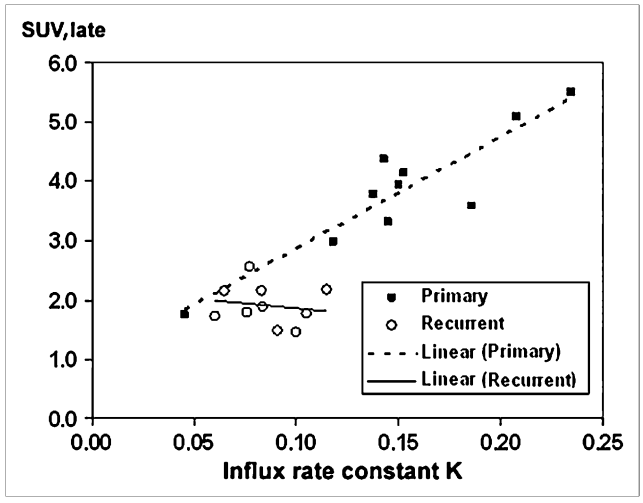

FIGURE 6. Scatter diagram of influx rate constant K in min^{-1} vs. 1-^{11}C-acetate uptake in prostate (SUV). Black squares indicate primary cancer and open circles indicate recurrent cancer. Lines are results of linear regression analysis, $r = 0.91$ (squares) and $r = -0.17$ (circles).

partial-volume effects can be performed on an individual basis. VOI generation may be simplified, by generating them directly from the high-resolution anatomic images, which are fused to the metabolic images. FA will remain important for the generation of the tumor time–activity curve, as it highlights the metabolically active, and presumably proliferating, part of the tumor (*29*). The thresholding algorithm selected the most active part of the tumor/prostate. Although there were no necrotic zones visible in our patients, it would be unlikely for necrotic tissue to have sufficient acetate uptake to reach half of the tumor maximum. The top half of voxels was selected to reduce fluctuations compared with the maximum SUV from 1 voxel—that is, leading to more reliable fitting and parameter estimation. Parameters derived from this part of the tumor turned out to correlate with the type of the neoplasm—that is, primary versus recurrent (Fig. 6). Further studies will be necessary to confirm these observations in larger patient groups.

Prostate Cancer Kinetics and Biology

A 3-compartment model with 3 parameters—that is, setting k_4 to 0 and neglecting the tissue blood volume term—with metabolite correction was sufficient to describe the acetate kinetics. This simplified model had overall the lowest error (WRSS) and AIC. In other words, when increasing the parameters from 3 to 4 or 5, there is no improvement in the AIC. Directly comparing the 3C-3p and 3C-5p models with the F test shows no significant differences in any of the patients. Apparently, an improved fit is a trade-off for including more parameters. The model with the lowest number of parameters is selected to prevent overfitting of the data.

Obviously, Patlak graphical analysis produced adequate estimates of the influx rate constant and distribution volume for prostate cancer (Tables 1 and 2). Figure 4 shows that primary prostate cancer had the highest transport rate constant k_1, and BPH was similar. Significant differences ($P < 0.01$) between primary and recurrent cancer were found for k_1, K, V_d, SUV-early, and SUV-late. The correlation between transport k_1 and influx K was high, 0.82 and 0.84, respectively (Fig. 5). A poor correlation was found between influx rate constant K and SUV for recurrent tumors (Fig. 6), suggesting that, in this case, acetate uptake does not provide a reasonable estimate of the influx rate constant K in clinical practice. Reasons for this poor correlation could be early detection of recurrence because of close follow up, changed anatomy leading to altered perfusion patterns in the former prostate bed, and technical factors such as partial volume. Recurrences in the prostate bed may be small and present as thin foci, making recovery of the activity difficult. Examining the correlation between SUV-late and the various parameters revealed a weak negative correlation with k_1 ($r = -0.24$) for recurrent tumors, whereas primary prostate cancer shows a positive correlation ($r = +0.74$). This supports the hypothesis that perfusion and, hence, transport are affected differently for each tumor type. Overall transport and metabolism of tracer—that is, influx rate K—shows a strong correlation with the transport rate k_1 for both tumor types (Fig. 5). Partial-volume effects alone cannot explain the differences between primary and recurrent tumors as found in Figure 6. Incomplete recovery of the blood activity would lead to an increase in k_1 and K. However, as a group, the size of the iliac vessels will be similar in men with primary versus those with recurrent cancer, and partial-volume effects on the input function should be the same. Average tumor size was also similar for both groups. Assuming a very inhomogeneous uptake in recurrent tumors, would lead to a lower recovery coefficient if compared with a more homogeneous group of primary tumors. However, although the parameters values would be lower, a positive correlation between influx and uptake would still be expected. The lack of such correlation in recurrent tumors suggests other reasons the than partial volume. The range of K is narrow (Fig. 6) and small sample size and selection of tumors could have contributed to the lack of correlation. On the other hand, biologic differences between primary and recurrent tumor cancer cells—that is, different membrane transport channels, altered TCA cycle, and so forth—might have caused this discrepancy. More research is warranted to elucidate these differences.

The acetate uptake in our subgroups was similar to those of Oyama et al. (*6*) for primary cancer, ranging from 3.3 to 9.9 SUV, compared with our 1.8–5.5 SUV. The higher numbers suggest more advanced disease in their population. They found a relationship between tumor grade and uptake. In our primary cancer group, 9 men had a T2 tumor and 1 had a T3 tumor, whereas the recurrent group was split evenly with 5 patients in each group having T2 and T3 tumors. The late uptake was slightly higher for T3 tumors with 2.2 compared with 1.9 for T2 tumors ($P = 0.2$). In the article of Oyama et al. on recurrent cancer (*7*), no uptake measures were provided, but our results show generally lower SUVs. Obviously, this is dependent on the time of discovering the PSA relapse. Because our patients were closely monitored, with a serum PSA test every 3–4 mo, the detection of recurrence was rather early, which might explain the lower uptake. This is corroborated by the PSA velocity, which is a measure of tumor burden. In 6 of 10 men with recurrent cancer, the PSA velocity was <0.3 mg/mL/mo. Oyama et al. (*6*) also found a relation between age and uptake. We had only 2 patients younger than 50-y-old. Surprisingly, the uptake in the men with BPH was higher for the 78-y-old (SUV 3.8) compared with the 49-y-old (SUV 3.2).

As was pointed out by van den Hoff (*17*), the transport constant k_1 is not equal to the tissue perfusion F, but to F/E, with E being the extraction fraction (Supplemental Appendix). In the myocardium, there is a steep drop-off of acetate during the initial minute. We did not observe this in our data; our initial sampling of 10 s per frame should have

been sufficient to measure such an early effect. The prostate time–activity curve shows a steep incline and reaches the plateau before 5 min. A myocardial time–activity curve, on the contrary, drops to <20% of its peak at 20 min. The acetate turnover and incorporation into lipids, amino acids, or steroids is too long to be measured in our 20-min time span. Therefore, the plateau-shaped time–activity curve in prostate cancers suggests retention of acetate in tissue. The sharp contrast between the curves of the prostate and the myocardium suggests that the model for the prostate proposed by Fricke et al. (*27*), based solely on increased citrate oxidation (*28*), is invalid. A plateau-shaped acetate uptake/retention curve has been reported for many other tissues, such as pancreas, salivary glands, bowel, as well as solid cancers and lymphoma (*4*). As reported by Kato et al. (*8*), the early uptake is the same as the late uptake, and the early-to-late uptake ratio is not significantly different from unity for any of the patients. The suggestion that the ratio is higher for primary prostate cancer and could be used for differentiation (*4*) is not supported by our data or those from Kato et al. (*8*). In this respect, prostate cancer behaves similarly to the behavior of normal prostate tissue. The finding that BPH cannot be differentiated from primary cancer (Fig. 4) has been reported for both ^{18}F-FDG and 1-^{11}C-acetate (*4*). The early-to-late acetate uptake ratio is equal to unity. This is in stark contrast with the myocardium, which shows a rapid decline, and 80% of the 1-^{11}C-label has disappeared by 20 min. The plateau curve suggests a prolonged retention of the 1-^{11}C-label in benign prostate cells.

Table 2 shows that k_2 and k_3 are similar for primary and recurrent tumors, whereas k_1 and K are different, providing a means to differentiate them. Whereas k_1 seems similar in primary and benign tumors, Table 2 suggests that k_3 is twice as high in malignant tumors as BPH. Although our numbers are too small for conclusions, one could hypothesize that k_3 might be able to differentiate between malignant and benign lesions. Table 2 shows that k_2 is the highest for malignant tumors, about twice as high as BPH, and that V_d is the lowest for malignant tumors, less than half of BPH. Increased oxidation of acetate through the TCA cycle is manifested as an increased k_2 or decreased V_d, which is the case in comparing malignant tumors versus BPH. This observation would be consistent with the work by Costello and Franklin (*28*), in which it was shown that, unlike normal prostate cells, which are citrate producing, prostate cancer cells are oxidizing cells (with increased Krebs cycle activity). Thus, it appears that k_2, k_3, or V_d might be able to discriminate benign from malignant tumors, whereas k_1 or K should help differentiate between primary and recurrent tumors. Further investigations to pursue these findings are warranted.

We did not find a correlation between SUV and influx rate constant K for recurrent tumors. Although our sample is too small for firm conclusions, this finding is troublesome because it suggests that the uptake cannot be used to "characterize" or "grade" the type of recurrence. This might suggest that therapy monitoring with 1-^{11}C-acetate is limited. For detection of recurrence, however, the presence or absence of acetate uptake is assessed and its utility in recurrent prostate cancer has been determined (*5,7,27*). After radical prostatectomy, either by surgery or radiation, no viable tissue is expected in the prostate bed. Thus, any acetate uptake in this region is considered to indicate recurrence of disease.

The field of view of our system is 16 cm, which is not suited for adequate lymph node imaging or staging. Four patients had a pathologic lymph node in the field of view, and 2 patients had a bone metastasis. Using the 3C-3p model, the kinetic parameters of the lymph nodes closely resembled those of the prostate cancer of the patient in question. The bone metastases, on the other hand, demonstrated a transport and influx constant twice as large as those of the corresponding prostate cancer. This latter finding might be interpreted as more aggressive behavior of the bone metastases than the primary tumor.

Study Limitations

The limitations of this study are the relatively small subgroups, heterogeneity of tumors, and different stages of disease. Despite small subgroups, robust effects were found for primary cancers, revealing both a significantly higher transport (k_1) and influx (K) compared with those of recurrent prostate cancer. A linear relationship between transport and influx was also found for primary prostate cancer but not for recurrent cancer. The selection of a constant recovery coefficient (0.6 for the iliac vessels and 1.0 for the tumor/prostate) does not represent individual variations and may cause differences in the parameter estimates k_1 and K. Individual correction for partial-volume effects—that is, PET/CT—would obviously be a superior approach. The main objective of our study was to describe the kinetics and to test the model structure. The standard model for ^{18}F-FDG, with its known applicability under clinical circumstances, appears appropriate for 1-^{11}C-acetate and could be reduced to 3 parameters by ignoring k_4 and V_b.

CONCLUSION

The acetate kinetics of prostate cancer are adequately described with a 3-compartment model, simplified to the 3 parameters k_1, k_2, and k_3, and including corrections for ^{11}C-CO_2 in blood and partial volume. FA provides image-derived blood clearance and tumor uptake curves that are user independent. Transport rate k_1 and influx rate K, as well as SUV-early and SUV-late, are significantly different for primary cancer compared with recurrent cancer. The high correlation ($r = 0.91$) between 1-^{11}C-acetate uptake in primary tumor and influx rate constant K indicates that simple uptake measurements (SUV) will be sufficient in clinical practice. The 2 men with BPH had parameters that resemble those of primary prostate cancer. K and SUV for

PSA relapse cancer, on the contrary, do not show a significant correlation.

REFERENCES

1. Schiepers C, Hoh CK, Seltzer MA, Phelps ME, Dahlbom M. Factor analysis for quantification of ^{11}C-acetate PET in primary prostate cancer [abstract]. *J Nucl Med.* 2000;41(suppl 5):100P.
2. Schiepers C, Hoh CK, Nuyts J, Wu HM, Phelps ME, Dahlbom M. Factor analysis in prostate cancer: delineation of organ structures and automatic generation of in- and output functions. *IEEE Trans Nucl Sci.* 2002;49:2338–2343.
3. Seltzer MA, Jahan SA, Sparks R, et al. Radiation dose estimates in humans for ^{11}C-acetate whole-body PET. *J Nucl Med.* 2004;45:1233–1236.
4. Dimitrakopoulou-Strauss A, Strauss LG. PET imaging of prostate cancer with ^{11}C-acetate. *J Nucl Med.* 2003;44:556–558.
5. Kotzerke J, Volkmer BG, Neumaier B, Gschwend JE, Hautmann RE, Reske SN. Carbon-11 acetate positron emission tomography can detect local recurrence of prostate cancer. *Eur J Nucl Med Mol Imaging.* 2002;29:1380–1384.
6. Oyama N, Akino H, Kanamaru H, et al. ^{11}C-Acetate PET imaging of prostate cancer. *J Nucl Med.* 2002;43:181–186.
7. Oyama N, Miller TR, Dehdashti F, et al. ^{11}C-Acetate PET imaging of prostate cancer: detection of recurrent disease at PSA relapse. *J Nucl Med.* 2003;44:549–555.
8. Kato T, Tsukamoto E, Kuge Y, et al. Accumulation of [^{11}C]acetate in normal prostate and benign prostatic hyperplasia: comparison with prostate cancer. *Eur J Nucl Med Mol Imaging.* 2002;29:1492–1495.
9. Effert PJ, Bares R, Handt S, Wolff JM, Bull U, Jakse G. Metabolic imaging of untreated prostate cancer by positron emission tomography with 18fluorine-labeled deoxyglucose. *J Urol.* 1996;155:994–998.
10. Kotzerke J, Prang J, Neumaier B, et al. Experience with carbon-11 choline positron emission tomography in prostate carcinoma. *Eur J Nucl Med.* 2000;27:1415–1419.
11. Kotzerke J, Gschwend JE, Neumaier B. PET for prostate cancer imaging: still a quandary or the ultimate solution? *J Nucl Med.* 2002;43:200–202.
12. Kotzerke J, Volkmer BG, Glatting G, et al. Intraindividual comparison of [^{11}C]acetate and [^{11}C]choline PET for detection of metastases of prostate cancer. *Nuklearmedizin.* 2003;42:25–30.
13. Lear JL. Relationship between myocardial clearance rates of carbon-11-acetate-derived radiolabel and oxidative metabolism: physiologic basis and clinical significance. *J Nucl Med.* 1991;32:1957–1960.
14. Ng CK, Huang SC, Schelbert HR, Buxton DB. Validation of a model for [1-^{11}C]acetate as a tracer of cardiac oxidative metabolism. *Am J Physiol.* 1994;266:H1304–H1315.
15. Buck A, Wolpers HG, Hutchins GD, et al. Effect of carbon-11-acetate recirculation on estimates of myocardial oxygen consumption by PET. *J Nucl Med.* 1991;32:1950–1957.
16. van den Hoff J, Burchert W, Wolpers HG, Meyer GJ, Hundeshagen H. A kinetic model for cardiac PET with [1-carbon-11]-acetate. *J Nucl Med.* 1996;37:521–529.
17. van den Hoff J. Methodologic aspects of myocardial blood flow quantification with 1-^{11}C-acetate PET. *J Nucl Med.* 2001;42:1438–1439.
18. Sciacca RR, Akinboboye O, Chou RL, Epstein S, Bergmann SR. Measurement of myocardial blood flow with PET using 1-^{11}C-acetate. *J Nucl Med.* 2001;42:63–70.
19. Patlak CS, Blasberg RG. Graphical evaluation of blood-to-brain transfer constants from multiple-time uptake data: generalizations. *J Cereb Blood Flow Metab.* 1985;5:584–590.
20. Oberdorfer F, Theobald A, Prenant C. Simple production of [1-carbon-11]acetate. *J Nucl Med.* 1996;37:341–342.
21. Davenport RJ, Dowsett K, Pike VW. A simple technique for the automated production of no-carrier-added [1-carbon-11]acetate. *Appl Radiat Isot.* 1997;48:1117–1120.
22. Nuyts J, Dupont P, Mortelmans L. Iterative reconstruction of transmission sinograms with low signal to noise ratio. Paper presented at: *2nd IEEE Workshop on Computer Intensive Methods in Control and Signal Processing: Can We Beat the Curse of Dimensionality?* August 28–30, 1996; Prague, Czech Republic.
23. Fessler J, Ficaro E, Clinthorne N, Lange K. Grouped-coordinate ascent algorithms for penalized likelihood transmission image reconstruction. *IEEE Trans Med Imaging.* 1997;16:166–175.
24. Hudson H, Larkin R. Accelerated image-reconstruction using ordered subsets of projection data. *IEEE Trans Med Imaging.* 1994;13:601–609.
25. Sun KT, Chen K, Huang SC, et al. Compartment model for measuring myocardial oxygen consumption using [1-^{11}C]acetate. *J Nucl Med.* 1997;38:459–466.
26. Porenta G, Cherry S, Czernin J, et al. Noninvasive determination of myocardial blood flow, oxygen consumption and efficiency in normal humans by carbon-11 acetate positron emission tomography imaging. *Eur J Nucl Med.* 1999;26:1465–1474.
27. Fricke E, Machtens S, Hofmann M, et al. Positron emission tomography with ^{11}C-acetate and ^{18}F-FDG in prostate cancer patients. *Eur J Nucl Med Mol Imaging.* 2003;30:607–611.
28. Costello LC, Franklin RB. Citrate metabolism of normal and malignant prostate epithelial cells. *Urology.* 1997;50:3–12.
29. Yoshimoto M, Waki A, Yonekura Y, et al. Characterization of acetate metabolism in tumor cells in relation to cell proliferation: acetate metabolism in tumor cells. *Nucl Med Biol.* 2001;28:117–122.
30. Phelps ME, Huang SC, Hoffman EJ, Selin C, Sokoloff L, Kuhl DE. Tomographic measurement of local cerebral glucose metabolic rate in humans with (F-18)2-fluoro-2-deoxy-D-glucose: validation of method. *Ann Neurol.* 1979;6:371–388.
31. Huang SC, Phelps ME, Hoffman EJ, Sideris K, Selin CJ, Kuhl DE. Noninvasive determination of local cerebral metabolic rate of glucose in man. *Am J Physiol.* 1980;238:E69–E82.
32. van den Hoff J, Burchert W, Borner AR, et al. [1-^{11}C]Acetate as a quantitative perfusion tracer in myocardial PET. *J Nucl Med.* 2001;42:1174–1182.
33. Draper NR, Smith H. *Applied Regression Analysis.* 2nd ed. New York, NY: John Wiley & Sons; 1981.
34. Landaw EM, DiStefano JJ 3rd. Multiexponential, multicompartmental, and noncompartmental modeling. II. Data analysis and statistical considerations. *Am J Physiol.* 1984;246:R665–R677.
35. Akaike H. A new look at the statistical model identification. *IEEE Trans Automat Contr.* 1974;19:716–723.
36. Wu HM, Hoh CK, Choi Y, et al. Factor analysis for extraction of blood time-activity curves in dynamic FDG-PET studies. *J Nucl Med.* 1995;36:1714–1722.
37. Schiepers C, Hoh CK, Dahlbom M, Wu HM, Phelps ME. Factor analysis for delineation of organ structures, creation of in- and output functions, and standardization of multicenter kinetic modeling. *Proc SPIE.* 1999;3661:1343–1350.
38. Woodbury J. Regulation of pH. In: Ruch TaP HD, ed. *Physiology and Biophysics.* Philadelphia, PA: Saunders; 1965:899–934.
39. Schiepers C, Chen W, Dahlbom M, Cloughesy T, Hoh CK, Huang SC. ^{18}F-Fluorothymidine kinetics of malignant brain tumors. *Eur J Nucl Med Mol Imaging.* 2007;34:1003–1011.